The Use of Optical Flow for Road Navigation

Andrea Giachetti, Marco Campani, and Vincent Torre

***Abstract*— This paper describes procedures for obtaining a reliable and dense optical flow from image sequences taken by a television (TV) camera mounted on a car moving in usual outdoor scenarios. The optical flow can be computed from these image sequences by using several techniques. Differential techniques to compute the optical flow do not provide adequate results, because of a poor texture in images and the presence of shocks and vibrations experienced by the TV camera during image acquisition. By using correlation based techniques and by correcting the optical flows for shocks and vibrations, useful sequences of optical flows can be obtained. When the car is moving along a flat road and the optical axis of the TV camera is parallel to the ground, the motion field is expected to be almost quadratic and have a specific structure. As a consequence the egomotion can be estimated from this optical flow and information on the speed and the angular velocity of the moving vehicle are obtained. By analyzing the optical flow it is possible to recover also a coarse segmentation of the flow, in which objects moving with a different speed are identified. By combining information from intensity edges a better localization of motion boundaries are obtained. These results suggest that the optical flow can be successfully used by a vision system for assisting a driver in a vehicle moving in usual streets and motorways.**

***Index Terms*— Egomotion recovery, optical flow, relative motion detection.**

I. Introduction

ROBOTS and autonomous vehicles receive and have to process sensory information coming from the surrounding world. A major sensory input is vision and it is a challenge for robotics to extract all the relevant information from road image sequences acquired by a television (TV) camera mounted on a robot or an autonomous vehicle. Several vehicles are already able to drive along outdoor scenes using vision, such as the VAMORS [1]–[4], the VITA II [5], [6] and CMU–NAVLAB vehicles [7], [8]. The vision systems of these vehicles are focused on the detection of those features necessary to control the steering position and the detection of obstacles. The control of the steering position is obtained by a feedback loop in which the vision system recognizes the road on the images by a color based pixel classification [7]–[9] or detects and tracks road features using edge detection [1]–[3], [5], [10]–[13] or template matching [14]. The detection of obstacles is performed by the use of active sensors such as laser scanners [7], [8], [11], tracking of vertical edges [1]–[3], [10], stereoscopic vision [15], [16] and motion parallax [17]. Some aspects of optical flow, such as divergence [18] or other features [19]–[21] for detecting and avoiding obstacles have also been proposed or used. These vision systems, however, do not aim at extracting all the dynamic information contained in a sequence of changing images, which is captured by the optical flow [22]–[28] and it is interesting to evaluate whether a complete analysis and a full use of the optical flow can be useful for the autonomous navigation.

The major aim of this paper is to evaluate the possibility of computing and using the optical flow from image sequences acquired by a TV camera mounted on a commercial vehicle driving along usual roads in the countryside or in the city center. In these circumstances the computation of optical flow has to cope with undesired motion of the TV camera due to the vibrations of the vehicle. As a consequence differential techniques to compute the optical flow, which usually provide satisfactory results when the camera is fixed or carefully displaced [27], [28], do not provide an adequate and dense optical flow. The primary aim of this paper is to show how to overcome this problem and how to obtain reasonable estimates of the absolute speed, angular velocity and radius of curvature of the vehicle trajectory respectively. The recovery of these parameters is performed assuming a flat road with the optical axis of the camera parallel to the ground. These hypotheses are used to build a motion model linking the optical flow to the egomotion parameters. Anomalities in the model are used to design strategies for the detection of obstacles and relative motions in the scene.

The paper is organized as follows: Section II analyzes the performances of optical flow estimators on road sequences. Section III presents the relevant mathematical background on the properties of the motion field of egomotion. Section IV shows how to recover the instantaneous and angular speed and the radius of curvature from road image sequences. Section V is dedicated to the recovery of relative motion. Finally advantages and disadvantages of the use of optical flow will be discussed and compared with other approaches to the analysis of image sequences.

These results have been presented in a short form at two recent conferences [29], [30].

II. Computing Optical Flow From Road Image Sequences

In the near future, many cars and vehicles will be equipped with a TV camera mounted on board, to control and assist their

Manuscript received May 15, 1995; revised February 24, 1996. This paper was supported in part by grants from ASI, the ESPRIT Projects SSS 6961 and Insight II, Progetto Finalizzato Transporti PROMETHEUS, and Progetto Finalizzato Robotica. This paper was recommended for publication by Associate Editor M. Hebert and Editor S. Salcudean upon evaluation of the reviewers' comments.

A. Giachetti is with the CRS4, Cagliari 09123, Italy.

M. Campani is with the Dipartimento di Fisica, Università di Genova and with the Unità di Ricerca di Genova, Istituto Nazionale per la Fisica della Materia (INFM), Genova 16146, Italy.

V. Torre is with the SISSA/ISAS, Trieste 34014, Italy.

Publisher Item Identifier S 1042-296X(98)01544-4.

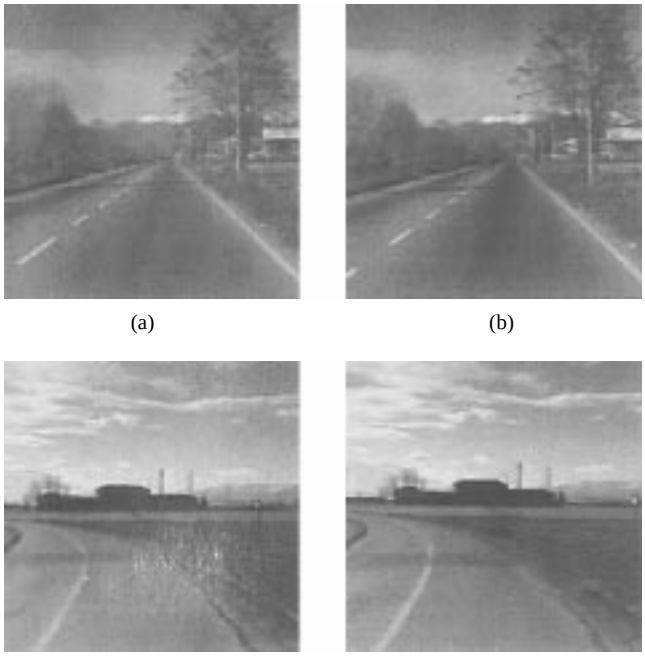

Fig. 1. Selected frames from image sequences acquired by a TV camera mounted on the moving vehicle: (a) and (b) images taken while the vehicle was moving along a straight road and in the absence of any relative motion, (c) and (d) as in (a) and (b) but while the vehicle was following a road turning to its left. Original images were composed by 512 × 512 pixels but only the central portion composed by 256 × 256 pixels was analyzed.

navigation. This imaging device provides image sequences, from which relevant information on the motion of the vehicle and on the presence of other moving vehicles can be extracted. Fig. 1 illustrates selected frames from image sequences analyzed in this paper and obtained while the vehicle is moving along a rectilinear way [(a) and (b)] or a road turning to the left [(c) and (d)].

Fig. 9 shows examples of relative motions, when another car is approaching the vehicle on the opposite lane [(a) and (b)] or overtaking it [(c) and (d)]. Our aim is to recover information on the vehicle egomotion, on the presence of other vehicles and their motion.

Many approaches to the analysis of image sequences compute an intermediate step, usually referred to as optical flow [22]–[26], [31]–[34]. Let us indicate with $E(x,y,t)$ the intensity at location (x,y) on the image plane of the imaging device at time t. Points on the image plane of the viewing device appear to move due to the presence of a relative motion between the viewing eye and the scene. The vector field $\vec{o}(x,y)$ of this apparent motion is usually called optical flow. The vector field does not usually coincide with, but is very similar to the two-dimensional (2-D) motion field $\vec{v}(x,y)$ [35], [36] which is the perspective projection on the image plane of the true three-dimensional (3-D) motion field produced by the relative motion between the viewing eye and the scene. Several techniques recover the optical flow $\vec{o}(x,y)$ from the intensity profile $E(x,y,t)$ and their performances have been compared on some selected image sequences [27], [28], [37] in which the viewing camera was usually fixed. Many of these techniques compute temporal and spatial derivatives of the intensity profile and are referred to as differential techniques. In comparison [27] a differential technique, developed in our laboratory, based on second order derivatives [38] provided satisfactory results also in comparison with the two best techniques. In comparison [28] another differential technique, also developed in our laboratory, based on the use of first order derivatives only [34] was ranked among the best available techniques to compute optical flow. Therefore we have tried to apply these techniques over road sequences.

Fig. 2(a) shows a typical sequence image taken from a vehicle moving on a flat straight road. The expected motion field has the qualitative form of (10) (see Section III) and is illustrated in Fig. 2(b). Fig. 2(c) illustrates the optical flow computed with the technique based on first order derivatives [34]. 5-points derivative masks were applied after a Gaussian spatial smoothing with $\sigma = 1.5$ pixels. The flow is blurred and even if the vectors have approximately the correct directions, they are strongly underestimated. With the technique based on second order derivatives [38] (still computed with five-point masks after spatial smoothing) only a few vectors are approximately correct [Fig. 2(d)].

These results show that differential techniques, which provide adequate results on test images, fail when applied to image sequences taken by a camera mounted on a moving car. Three factors contribute to the poor performances of these algorithms.

1) *Large displacements between consecutive frames*: When the car moves at a speed higher than 30 km/h, points in the image may move by more than than five pixels. As a consequence, aliasing in the computation of the temporal derivatives will introduce errors in the computation of optical flow [39]. Aliasing may be reduced by smoothing images or introducing a multi-scale decomposition [39]. Fig. 2(e) shows an optical flow computed from first order derivatives with a multi-scale technique [39]. The results is moderately better: vectors are still underestimated and unreliable in several regions due to other errors described in the following.
2) *Lack of texture*: Large portions of these images represent the road bed, where gray level variations are small. This lack of texture introduces significant instability also in the computation of spatial derivatives [39].
3) *Shocks and vibrations*: In road image sequences the image motion is not only caused by the egomotion of the car, but also by shocks and vibrations experienced by the car. Shocks and vibrations can introduce large and very rapid transients, with global displacements of the order of 1 pixel and frequencies of the order of 1 frame^{-1}. This high frequency component is a significant source of error in the computation of temporal derivatives.

It should be observed that most image sequences here analyzed were obtained with an imaging device carefully bolted to the vehicle. In other experiments the TV camera was secured to the vehicle less carefully and the amplitude of shocks and vibrations could be two to ten times larger. Shocks and vibrations responsible for the failure of differential techniques are very minute and difficult to eliminate mechan-

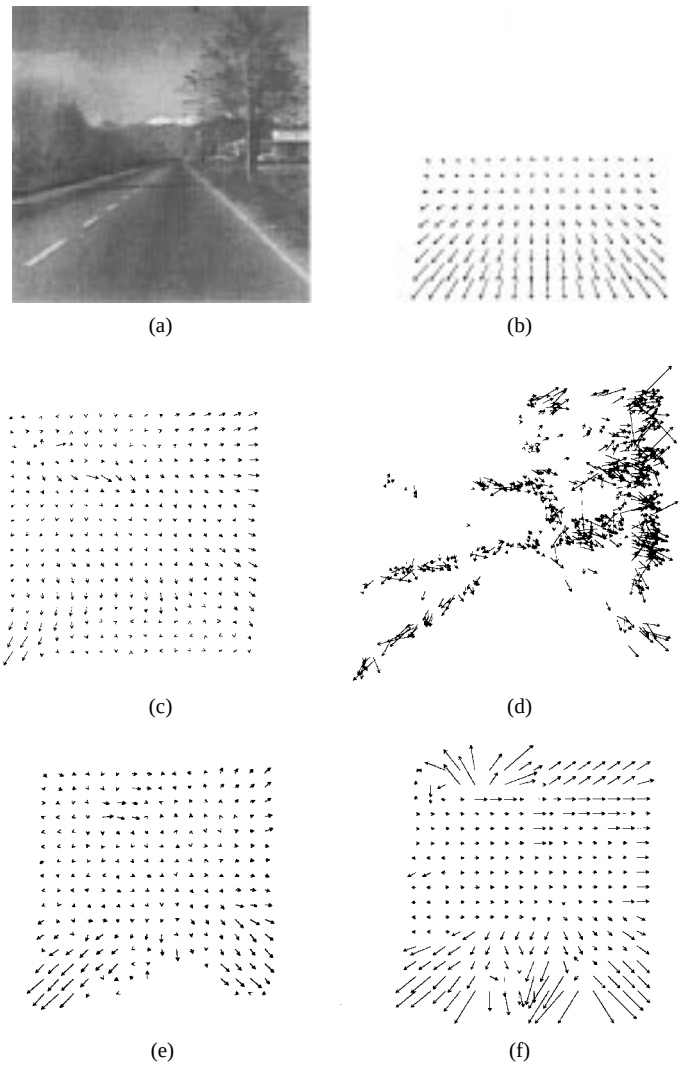

Fig. 2. Comparison of optical flows computed with different procedures, (a) a frame of the image sequence, (b) the theoretical optical flow expected from a pure translation over a flat surface, (c) optical flow computed with the technique described in [34] using first-order derivatives after a spatial smoothing of the images with $\sigma = 1.5$, (d) optical flow computed with the technique described in [38], using second-order derivatives. Only the reliable vectors are printed, (e) optical flow computed with a multiscale differential technique [39]. Vectors are still underestimated in several regions, (f) optical flow computed with the correlation technique. The size of the patches was 41×41 pixels and low-pass filtering was performed with a Gaussian filter with $\sigma = 1.5$.

ically. We therefore decided to use a correlation technique to compute the flow, searching the shift maximizing the correlation between the gray level pattern around each point between two consecutive frames. The point (x', y') at time t_2 corresponding to a point (x, y) at time t_1 minimizes the distance measure

$$\sum_{i=-n}^{n} \sum_{j=-n}^{n} (E(i+x', j+y', t_2) - E(i+x, j+y, t_1))^2. \quad (1)$$

This procedure may be quite expensive in terms of computing power and several assumptions can be made to speed up the computation. Firstly, the optical flow is not computed over the entire image composed by 256×256 pixels but on a less dense grid of 64×64 pixels. Secondly it is possible to speed up the computation by subsampling the windows used to compute the distance. In order to refine the algorithm precision, the point (x', y') at time t_2 corresponding to point (x, y) at time t_1 is chosen as the weighted center of the points at time t_2 with the lowest value of the quantity (1). Another improvement consists in a simple smoothing of the images with a Gaussian filter $\exp(-(x^2 + y^2)/2\sigma^2)$ with a value of 1.5 pixels for σ. The resulting correlation procedure usually provided a sufficiently dense and reliable optical flow.

It is evident that a correlation technique does not require the computation of spatial and temporal derivatives and therefore is less sensitive to the three sources of error described before.

III. The Motion Field of Egomotion

This section presents some mathematical properties of the 2-D motion field $\vec{v}$, which will be used for the estimation of egomotion; basic assumptions are that the vehicle is moving over a flat ground, that the instantaneous translation is parallel to the ground and that the angular velocity is perpendicular to the ground plane. These assumptions, usually referred to as passive navigation [36] greatly simplify the mathematical analysis. Moreover the structure of the 2-D motion field $\vec{s}$ caused by shocks and vibrations will be discussed.

Let us consider the system of reference $(0, e_1, e_2, e_3)$ solid with the viewing camera, as shown in Fig. 3, with its optical axis solid to the $\vec{e_3}$ axis. The image plane has equation $Z = f$, where f is the focal length of the imaging device. The perspective projection over the image plane of a point $\vec{X} = (X, Y, Z)$ in 3-D space is given by

$$\vec{x} = f\frac{\vec{X}}{Z} \quad (2)$$

and 3-D velocity vectors $\vec{V}$ are transformed into a 2-D motion field $\vec{v}$ using the relation

$$\vec{v} = \frac{f}{Z^2}[\hat{e_3} \times (\vec{V} \times \vec{X})]. \quad (3)$$

Considering rigid objects, the relative motion between the camera and the scene can be described by a translation $\vec{T}$ and a rotation $\vec{\omega}$ around an arbitrary axis $\vec{\gamma}$. In the case of passive navigation the instantaneous velocity can be assumed to be described by a pure rotation around a particular axis and the 3-D velocity becomes

$$\vec{V} = \vec{\omega} \times \vec{\rho} \quad (4)$$

where $|\omega|$ is the angular speed and $|\vec{\rho}|$ is the instantaneous radius of curvature. If the scene can be modeled as a plane, it is well known that the 2-D motion field on the image plane becomes

$$\begin{aligned} v_x &= c_{13}x^2 + c_{23}xy + (c_{33} - c_{11})fx - c_{21}fy - c_{31}f^2 \\ v_y &= c_{13}xy + c_{23}y^2 + (c_{33} - c_{22})fy - c_{12}fx - c_{32}f^2 \end{aligned} \quad (5)$$

where

$$c_{ij} = \frac{1}{fd(t)}(d(t)\vec{\omega} \cdot \hat{e_j} \times \hat{e_i} - \gamma_i V_j). \quad (6)$$

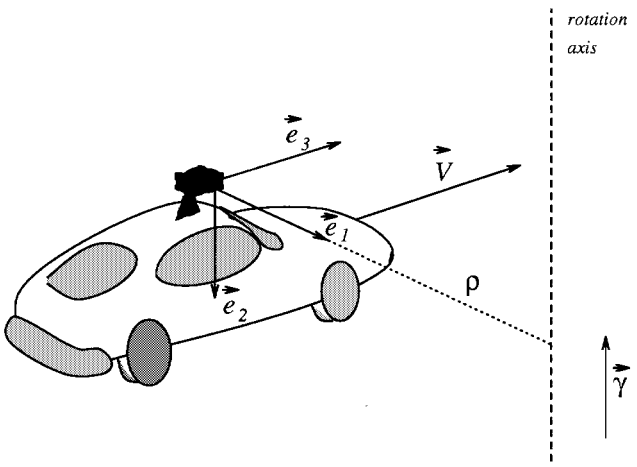

Fig. 3. The system of reference (e_1, e_2, e_3) solid to the TV camera mounted on the vehicle. The egomotion is described by the instantaneous speed V along $\vec{e_3}$ and the rotation $\vec{\omega}$ around the axis $\hat{\gamma}$, distant ρ from the TV camera. ρ is also the instantaneous radius of curvature.

Let us now suppose that $\vec{V}$ is always parallel to the optical axis and that the viewed plane is orthogonal to the image plane so that $\vec{V} = (0, 0, V)$ and $\hat{\gamma} = (0, -1, 0)$. The distance $d(t)$ between the viewed plane and the optical center is now a constant that identifies the height of the camera h from the ground plane. The 2-D motion field of (4) then becomes

$$\begin{aligned} v_x &= \frac{\omega}{f}x^2 + \frac{V}{hf}xy + \omega f \\ v_y &= \frac{\omega}{f}xy + \frac{V}{hf}y^2. \end{aligned} \tag{7}$$

The 2-D motion field of (7) is correct when the vehicle moves on a flat road through a flat landscape orthogonal to the image plane. As a consequence (7) can be assumed to be a good approximation of the true 2-D motion field when the vehicle moves on a flat road (such as in Fig. 1). A similar equation can be introduced for the motion field in the presence vertical buildings, orthogonal to the image plane [such as in Fig. 17(a)]. In this case, however, the distance between the building and the optical axis is unknown and the egomotion paramenters cannot be recovered.

Some useful observations on (7) can be made. As the focal length f is assumed to be known, the expected motion field depends on the two quantities ω, the angular speed, and V, the instantaneous speed. These two quantities are easily related to the instantaneous radius of curvature ρ by $V = \omega\rho$. Equation (7) can be rewritten as

$$\begin{aligned} v_x &= ax^2 + bxy + af^2 \\ v_y &= axy + by^2 \end{aligned} \tag{8}$$

where

$$\begin{aligned} a &= \frac{\omega}{f} \\ b &= \frac{V}{hf} \end{aligned} \tag{9}$$

and the two unknown quantities a and b can be clearly recovered from just one component of the motion field, as already shown [40]. In the case of a pure translation (8) simplifies to

$$\begin{aligned} v_x &= bxy \\ v_y &= by^2. \end{aligned} \tag{10}$$

A. The Motion Field of Shocks

Let us suppose that at time t the shock can be modeled as an instantaneous translation along the vertical axis T_y and a rotation ω_x along the axis e_1. The resulting motion field $\vec{s} = (s_x, s_y)$ is

$$s_x = \frac{\omega_x}{f}xy \tag{11}$$

$$s_y = \frac{T_y y}{h} + \frac{\omega_x}{f}y^2 + \omega_x f. \tag{12}$$

Now the order of magnitude of these terms should be evaluated. The next section will show that in our experimental imaging system the order of magnitude of the constant term $\omega_x f$ is about 1 pixel/frame. For the quadratic term, as f is about 350 pixels, we have

$$\frac{\omega_x}{f} \sim 10^{-4} \div 10^{-5} \text{ pixel}^{-1} \text{ frame} \tag{13}$$

and being y^2 at most $\sim 10^4$ near image borders, this term is not too relevant. For the linear term, with a camera height of about 1 to 2 m for a value of $T_y \sim 1$ cm/s, we have

$$\frac{T_y}{h} \sim 10^{-3} \text{ frame}^{-1} \tag{14}$$

and being y at most 10^2 pixels near the image borders, $T_y y/h \ll 1$ pixel/frame. As a consequence the constant term appears to be predominant. If shocks also produce a rotation ω_y around the e_2 axis and a horizontal translation T_x, by a similar analysis we reach the conclusion that the predominant terms of the motion field produced by shocks and vibrations are two constant terms in the vertical and horizontal direction. When the TV camera is mounted on a vehicle moving on a rugged road, the model of the 2-D motion field of disturbances cannot be approximated as two constant terms. In this case, in order to recover the egomotion, an extensive use of Kalman filters is useful.

IV. The Recovery of Egomotion

In this section we will discuss how to estimate the egomotion from image sequences obtained by a TV camera mounted on a moving vehicle. The proposed procedures are composed by two steps: first optical flows are computed and corrected for shocks and vibrations (see Section IV-A) and then motion parameters are recovered from corrected optical flows (see Section IV-B). A temporal filtering of the computed parameters is also introduced (see Section IV-C). The correlation procedure described in Section II provides a dense optical flow. However not all vectors are reliable and we have introduced a procedure to remove those which have been obtained by a high value of the distance measure (1). These

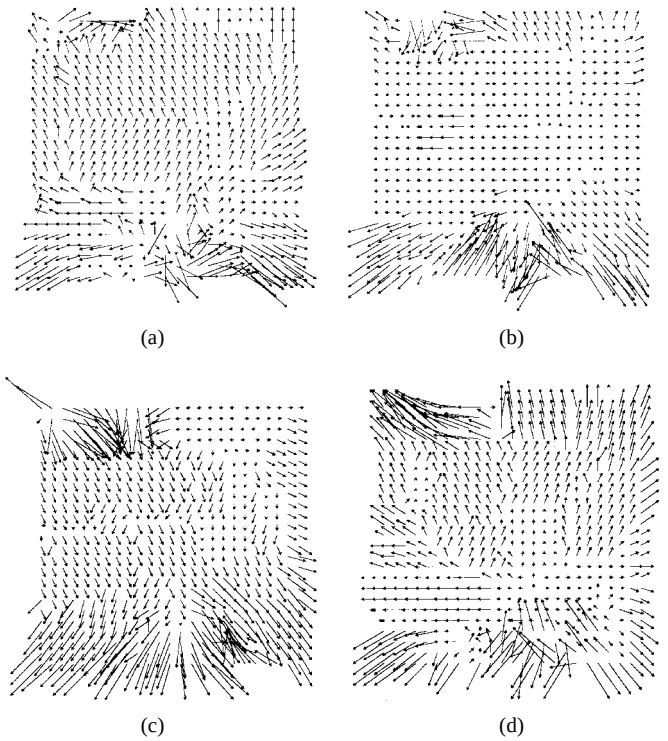

Fig. 4. (a)–(d) four optical flows computed with the correlation technique from an image sequence taken while the vehicle was moving in a rectilinear way [see Fig. 1(a) and (b)] in the absence of any other vehicle. Observe in (a), (c), and (d) the downwards and upwards deflections of vectors caused by shocks. Only the optical flow in (b) has broadly the flow expected from a pure translation.

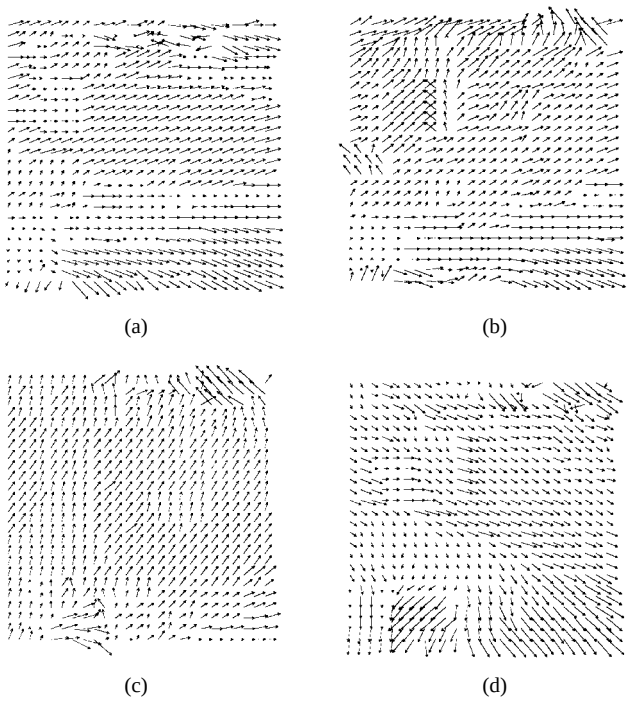

Fig. 5. (a)–(d) Four optical flows computed with a correlation technique from an image sequence taken while the vehicle was moving in a curvilinear way [see Fig. 1(c) and (d)]. Observe in (c) the upwards deflections of vectors caused by shocks.

vectors are not used neither for shock compensation nor for the motion parameters estimation here described.

Fig. 4 reproduces four optical flows obtained from different pairs of images of a sequence where the vehicle was moving along a straight road and no other vehicles were present. Almost none of the optical flows in Fig. 4 has the form expected from a pure translation [see Fig. 2(b)].

Optical flows computed from different pairs of images of a sequence acquired when the vehicle was moving along a curved road are shown in Fig. 5. These flows do not have the structure expected in the case of passive navigation, where a singular point on the line $y = 0$ is expected. The optical flows reproduced in Figs. 4 and 5 show random upwards and downwards global deflections. These unexpected movements of the camera add new terms to the motion field.

As shown in the previous section, a better model of the expected 2-D motion field at a given time t is

$$\begin{aligned} v_x &= ax^2 + bxy + af^2 + s_x \\ v_y &= axy + by^2 + s_y \end{aligned} \tag{15}$$

where the effect of shocks is described by the addition of two parameters s_x and s_y, both independent of $\vec{x}$. a and b are expected to vary smoothly with time, while s_x and s_y are random variables describing the noise introduced by shocks and vibrations and are almost uncorrelated. An estimate of s_x and s_y is necessary for the recovery of egomotion parameters. When the vehicle moves in a rectilinear way along a straight road the motion field [see (10)] is expected to be very small around the center of the image. As a consequence an estimate of s_x and s_y can be obtained by computing the average displacement of the obtained optical flow in an area around the center of the image $(41 \times 41$ pixels).

Fig. 6 reproduces the estimated values of s_x (A) and s_y (B) in the image sequence shown in Fig. 2(a). s_x and s_y appear to be random variables almost uncorrelated with a mean value of .04 and $-.07$ pixels/frame and a standard deviation of .45 and .75 pixels/frame, respectively. In image sequences obtained using the same TV camera mounted on a high quality stabilized platform on the same vehicle and day, the mean square of the horizontal shock was usually half of the vertical shock. These quantities refer to a given set of image sequences and the estimates of s_x and s_y with other vehicles and a different mounting of the TV camera provided different results. The amplitude of shocks and vibrations is clearly an intrinsic property of the road, the vehicle and also the driver's temperament and cannot be unequivocally estimated *a priori*. When the viewing camera was mounted on a commercial vehicle moving on a rugged road and could experience the same shocks and vibrations as the driver, the values of s_x and s_y could be as large as 10 pixels/frame.

A. Shock Cmpensation: Optical Flow Correction

It is evident that the image motion is the sum of a smooth component due to the car egomotion and a high frequency component due to the camera vibrations. A spatio-temporal smoothing may reduce the effect of shocks. However, the use of some procedures for image stabilization may be advantageous. For instance, image stabilization can be obtained by detecting a dominant motion and subsequently extracting

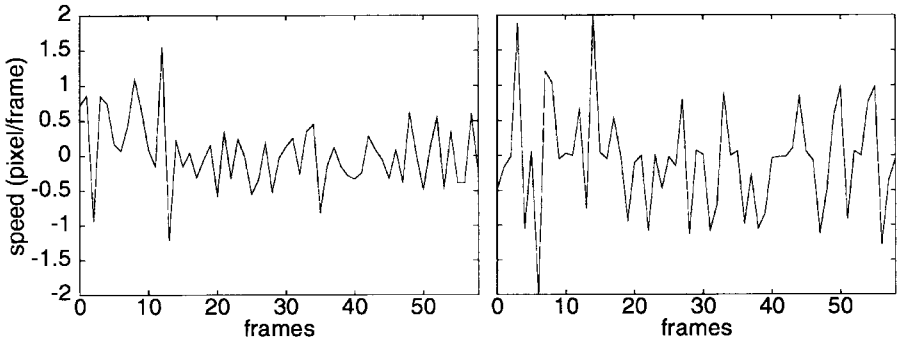

(a) (b)

Fig. 6. An estimate of vertical and horizontal shocks from the image sequence of Fig. 1(a) and (b): (a) horizontal shocks, and (b) vertical shocks. The average estimated horizontal and vertical shocks were 0.04 and -0.07 pixels, respectively, and the standard deviations were 0.45 and 0.8 pixels, respectively.

the local motion after compensation [41], [42]. Our case is different: indeed, we do not have to separate a local motion from a background motion, but to separate two fields superimposed almost everywhere. In order to do so, we have analyzed the theoretical motion fields due to the car egomotion and to the camera vibrations. In the case of passive navigation and if the optical axis is parallel to the ground, the motion field around the horizon, assumed to be located in the image plane near the line $y = 0$, is expected to have a vertical component equal to zero [see (7)]. Therefore an estimate of s_y is the average vertical displacement $\langle s_y \rangle$ in the strip between the two lines $y = -c$ and $y = c$. As a consequence a possible compensation for shocks and vibrations can be obtained by computing the value $\langle s_y \rangle$ in each flow and then subtracting $\langle s_y \rangle$ from the original flows. A similar estimate cannot be obtained for s_x, as in the general case of passive navigation the horizontal component of the flow along the line $y = 0$ is not necessarily zero. However, in many cases (see Fig. 6), the average horizontal shock was found to be smaller than the vertical shock and could often be neglected. The effect of correcting the original flows of Fig. 4 is shown in Fig. 7. As the flow above the horizon, corresponding to the sky, is not usually much reliable, only the half lower part of the flow is considered. These corrected optical flows have the structure expected from a rectilinear translation [compare with the flow of Fig. 2(b)]. Similarly after correction, the flows of Fig. 5, have a global structure, shown in Fig. 8, which is much closer to that expected in the case of passive navigation.

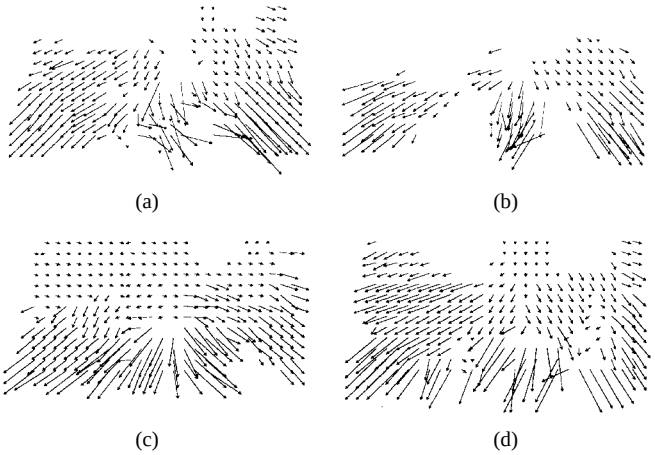

(a) (b) (c) (d)

Fig. 7. The optical flows shown in Fig. 4 after correction. The average vertical displacement around the horizon (in a strip between $y = -10$ pixels and $y = 10$ pixels) was subtracted from the original optical flow. Only the optical flows below the horizon are considered.

B. Recovery of Egomotion

Given the model of egomotion represented by (7), the recovery of egomotion implies the estimation of the two parameters ω and V from the corrected optical flows.

We have analyzed three different methods: the first one is to be used only in the case of rectilinear motion (Method 1) and the other two (Method 2 and 3) for the general case.

1) Method 1: Method 1 assumes that the vehicle is moving by a pure translation so that the parameter ω is equal to 0 and only V must be estimated. This method provides better results with a double fit procedure: the corrected optical flow is fitted with (10) and an estimate of V is obtained; then all vectors which significantly differ from the values obtained using (10), with V equal to the first estimate, are discarded and a second fit of the remaining vectors is performed with (10).

2) Method 2: Method 2 first estimates ω by computing the average horizontal displacement along the vertical axis $x = 0$. When this estimate of ω is obtained, V is estimated from each flow vector through the equation:

$$V = \frac{v_y h f}{y^2} - \frac{\omega h x}{y} \tag{16}$$

that follows immediately from (7). The values of V are then averaged in three regions roughly corresponding to the right, center and left lower part of the image. The final estimate of V is that obtained in the region where the estimate variance was the smallest.

3) Method 3: Method 3 simultaneously estimates ω and V in the three regions (left, center and right). As in Method 2 the final estimate is that obtained from the region with the smallest variance.

C. Temporal Filtering

The parameters computed with these methods are not always reliable. Components of shocks not compensated and erroneous flow vectors may cause large errors in the estimates of $\vec{V}, \rho, \omega$. These errors can be reduced by filtering the output.

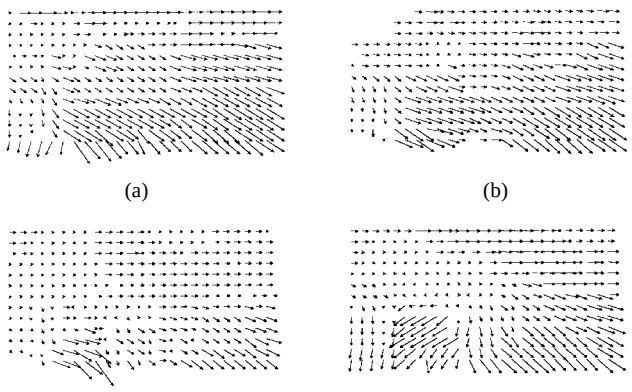

Fig. 8. The same optical flows as in Fig. 5 after correction. The average vertical displacement around the horizon was subtracted from the original optical flow. Only the optical flow below the horizon is considered.

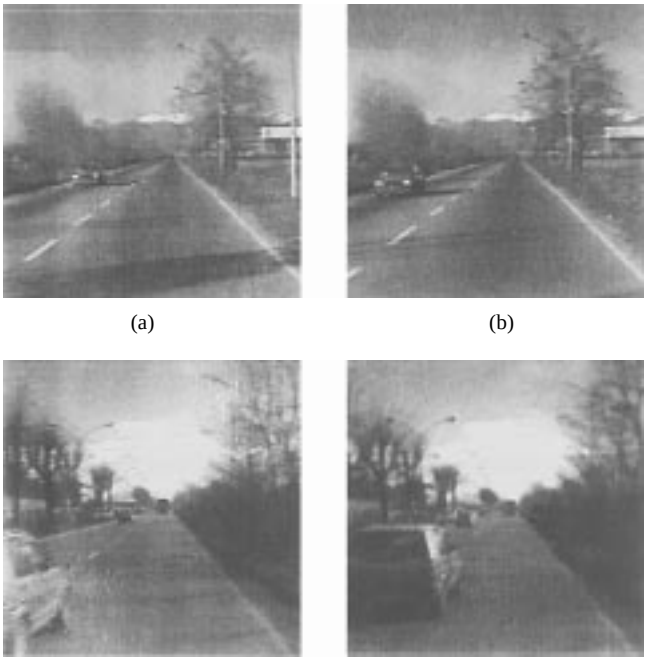

Fig. 9. Examples of relative motions: (a) and (b) the vehicle moves straightforward and another vehicle is approaching on the other lane and (c) and (d) the vehicle moves straight forward and another vehicle is overtaking.

If $\mathrm{in}(t)$ is the estimate of a motion parameter at time t, the filtered estimate $\mathrm{out}(t)$ is defined by

$$\mathrm{out}(t) = \frac{a+\delta(t)}{a+b+\delta(t)}\,\mathrm{out}(t-1) + \frac{b}{a+b+\delta(t)}\,\mathrm{in}(t) \quad (17)$$

where $\delta(t)$ is an estimate of the error of the instantaneous measurement. The filter of (17) can be considered a Kalman filter with b as the prediction error and $\delta(t)+a$ the error measurement. $\delta(t)$ was estimated as the average vertical flow near the horizon at time t before the correction. Best performances were obtained with values of 3 and 1 for a and b respectively.

D. Experimental Results

The algorithms for the egomotion recovery have been tested on several image sequences. Ground truth values of the speed were obtained from on-board instrumentation and in some cases were checked by measuring the length of road markers. Ground truth values of the angular velocity or radius of curvature were not available.

1) Comparison of the Three Methods: Fig. 10 illustrates a comparison among the three Methods for a case of rectilinear motion [sequence of Fig. 1(a)]. The first, second and third rows correspond to Methods 1, 2, and 3 respectively. The angular speed ω was estimated only from Methods 2 and 3 [see (d) and (f)]. The broken lines indicate the raw estimate and the continuous lines represent a smoothing after the temporal filtering. All three methods provide an average instantaneous speed of about 35 Km/h, consistent with the reading of on board instruments (38 Km/h). Method 2 gave an average angular speed around zero, while Method 3 gave an erroneous average angular speed of about .01 rad/s. The results provided by Methods 2 and 3 in the case of the curvilinear motion [see Fig. 1(c) and (d)] are shown in Fig. 11. The first and second columns refer to Method 2 and 3, respectively. Both Methods estimate the instantaneous speed around 35 Km/hr [(a) and (b)], the angular speed around .06 rad/s [(c) and (d)] and the radius of curvature around 180 m [(e) and (f)]. These estimates are in agreement with the direct measurement of these quantities.

A total of 15 image sequences were analyzed and good results were obtained. The comparison of the speed computed (with Method 2) on 15 sequences with the ground truth values is shown in Fig. 12. The correlation of the data is satisfactory.

2) Large Shocks and Estimates Without Flow Correction: The recovery of egomotion parameters presented in IV-A and IV-B was based on the use of corrected optical flows. The proposed correction was feasible only when the horizontal shocks could be neglected, which is not the case in the presence of large shocks when the vehicle is moving on a rugged road or when the camera experiences vibrations produced by the engine. Temporal filtering allows however the recovery of egomotion parameters from raw optical flows. Fig. 13(a) illustrates a frame from another series of image sequences in which the viewing camera was tightly bolted on a commercially available vehicle, moving in the city center of Genoa. Because of the bumpiness of the road, even when the vehicle was moving along a rectilinear road, the computed optical flow had large oblique deflections, as shown in Fig. 13(b). In this case the motion field $\vec{s}$ of shocks and vibrations had a significant horizontal component.

Fig. 13(c) illustrates the instantaneous estimates of the vehicle speed. The vehicle was moving at about 35 km/h and the instantaneous estimates could be wrong by even 200%. If the filter is applied to the flow estimation, a reasonable estimate is obtained after about 10 to 20 frames, depending on the parameters choice. must be chosen. Fig. 13(d) reproduces the filtering of the data of Fig. 13(c) with the values $a = 3$, $b = 1$ (dotted line), $a = 6$, $b = 1$ (broken line) and $a = 9$, $b = 1$ (continuous line).

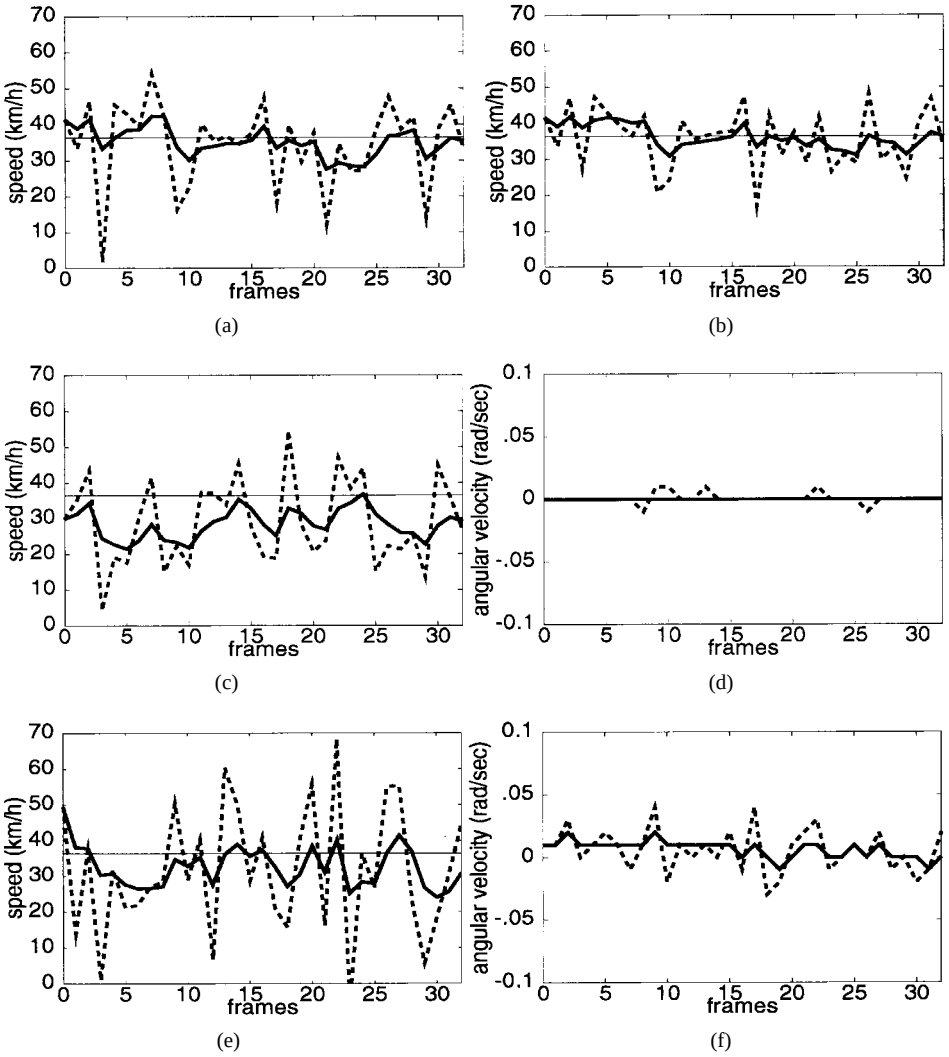

Fig. 10. Comparison among the three methods described in the text to recover the egomotion parameters from the flows of Fig. 7. Data shown in the first row were obtained with Method 1 after one fit (first column) and after two fits (second column). Data shown in the second and third rows were obtained with Methods 2 and 3 discussed in the text. The first column refers to the recovery of the instantaneous speed V and the second column to the recovery of the angular speed ω. The broken line is the instantaneous estimate and the solid thick line is the estimate obtained with the temporal filter. a and b were set equal to 3 and 1, respectively. The thin straight lines in (a), (b), (c), and (e) represent the ground truth values.

V. The Recovery of Relative Motion

After recovering an estimate of the egomotion, information on the presence of other moving vehicles either approaching [see Fig. 9(a) and (b)] or departing [see Fig. 9(c) and (d)] should be obtained. In this section, methods for detecting and localize relative motions are illustrated. First it is shown how to detect the presence of a relative motion by analyzing the speed estimates obtained in specific regions with the methods previously described (Section V-A). Then a coarse segmentation of obstacles based on the optical flow map (Section V-B) is illustrated. Finally a refinement of the obstacle localization exploiting information coming from intensity edges is described (Section V-C).

A. Detection of Relative Motion

The motion of vehicles approaching at an opposite speed will produce a diverging flow on the image plane which is qualitatively similar to that caused by the egomotion of the vehicle. However the diverging flow, produced by the combination of the egomotion and the relative motion of the other vehicle, can be quantitatively distinguished from the flow caused by the egomotion. On the contrary the motion of a vehicle departing or overtaking, will produce a converging flow which is qualitatively different from that expected from egomotion. These observations will be used to detect and distinguish among these relative motions. Fig. 14 illustrates two optical flows [(a) and (b)] computed from the image sequence of Fig. 9(a) and (b). The corrected optical flows are shown in Fig. 9(c) and (d). These flows have roughly the form expected from a pure translation, but vectors on the left appear to be larger than those on the right, thus suggesting the presence of another vehicle moving in the opposite direction. Fig. 15 illustrates two optical flows [(a) and (b)] and the corresponding corrected flows [(c) and (d)] when another vehicle is overtaking [see Fig. 9(c) and (d)]. These optical flows are qualitatively different from those shown in Fig. 14. The flow is converging in the left region and diverging in the right region, thus indicating the presence of another

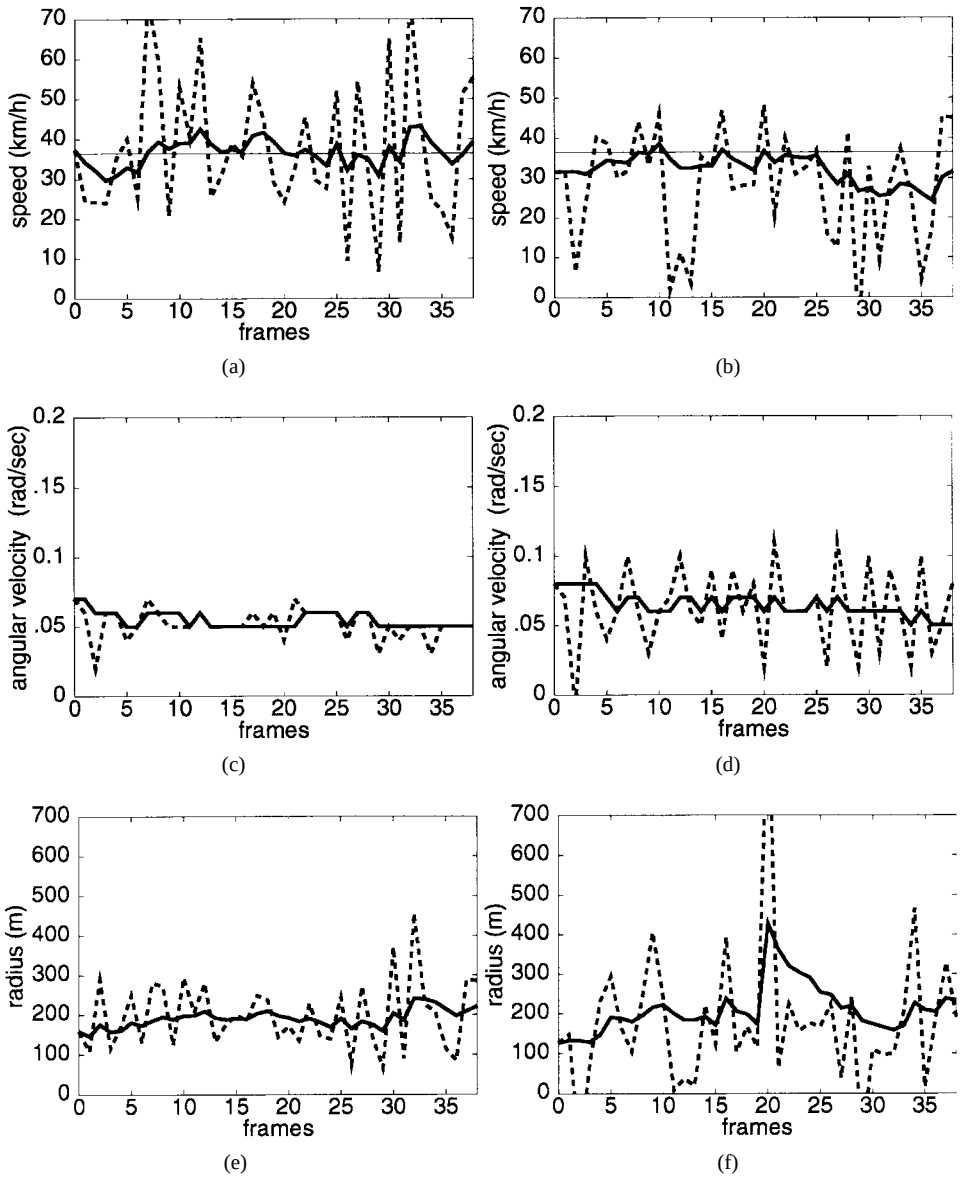

Fig. 11. Comparison between Methods 2 (first column) and 3 (second column) illustrated in the text, to recover the egomotion parameters from the flows of Fig. 8: instantaneous speed V (a) and (b), angular speed (c) and (d) and radius of curvature ϱ (e) and (f). The broken line is the instantaneous estimate and the solid thick line is the estimate obtained with the temporal filter. The thin straight lines in (a) and (b) represent the ground truth value.

vehicle moving in the same direction but at a greater speed. These relative motions can be quantified by estimating and comparing the value of V obtained with Methods 1 and 2 in the right and left region. Fig. 16 reproduces the computed speed in the left (solid line) and right region (broken line). Methods 1 and 2 were used to obtain the estimates shown in the first and second row respectively. The first and second columns refer to the flows of Figs. 14 and 15, respectively. When another vehicle is approaching the estimated speed in the right region is transiently larger than that in the left region [(a) and (c)]. In the case of a car overtaking, the instantaneous speed in the right region may become negative [(b) and (d)]. The detection of these relative motions was successful in the seven image sequences analyzed. The proposed technique to compute the optical flow is able to detect and broadly localize motion boundaries associated to the relative motion, but cannot provide a precise segmentation of different moving objects.

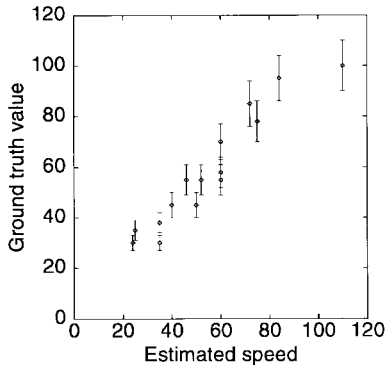

Fig. 12. Estimated speed versus ground truth values for 15 sequences after filter stabilization. The ground truth value of the speed was obtained from the on-board instrumentation, which is precise within 10%.

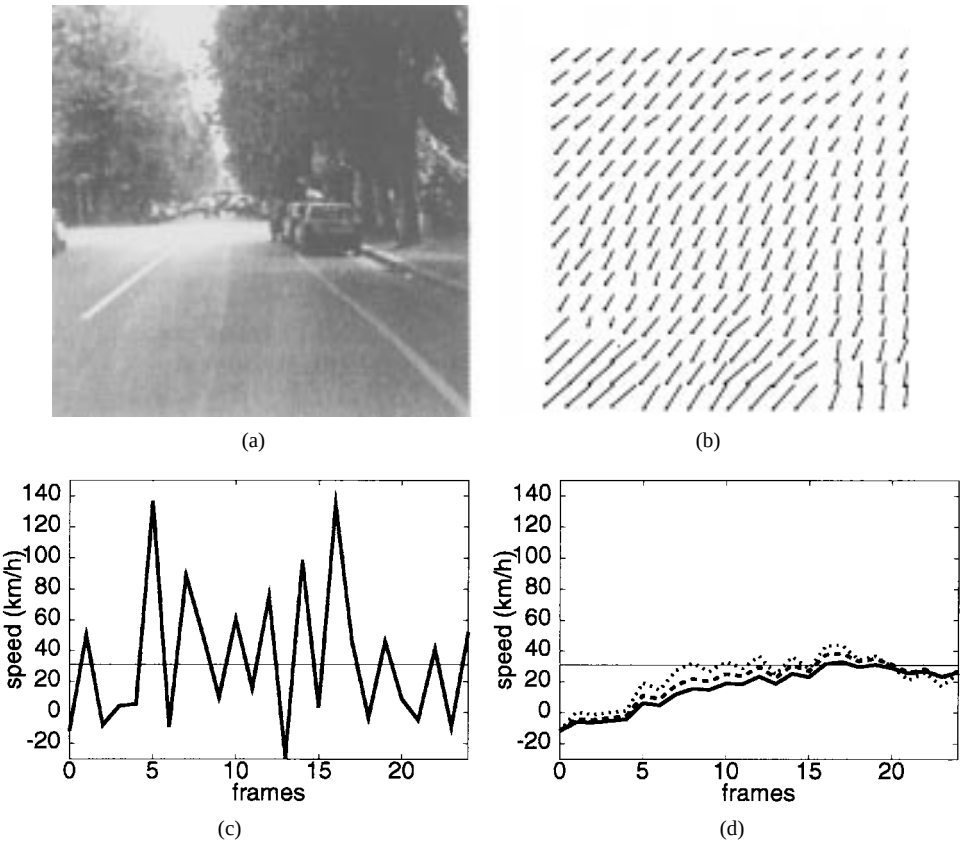

Fig. 13. The recovery of egomotion from raw optical flows: (a) frame from an image sequence acquired in the city center of Genoa, (b) example of an optical flow computed with the correlation algorithm, (c) the instantaneous estimates of V, and (d) data filtered as described in section IV-C with different parameters: $a = 3$, $b = 1$ (dotted line), $a = 6$, $b = 1$ (broken line) and $a = 9$, $b = 1$ (continuous line). The thin straight lines represent the ground truth value.

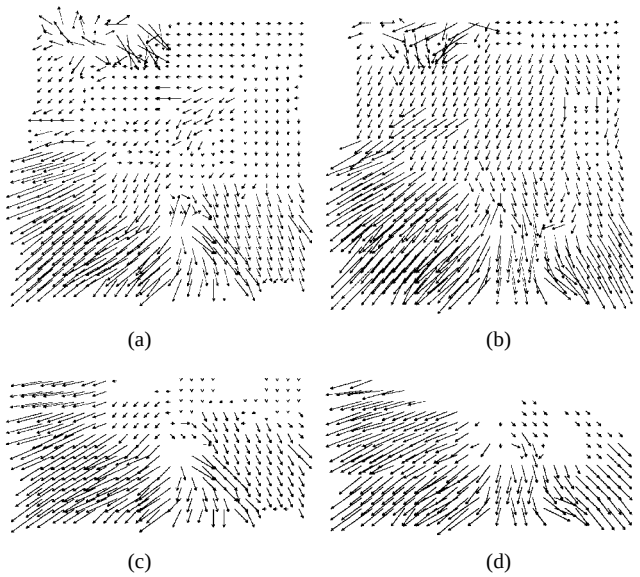

Fig. 14. The optical flows of relative motion when another vehicle is approaching on the other lane: (a) and (b) are raw optical flows, and (c) and (d) are corrected optical flows.

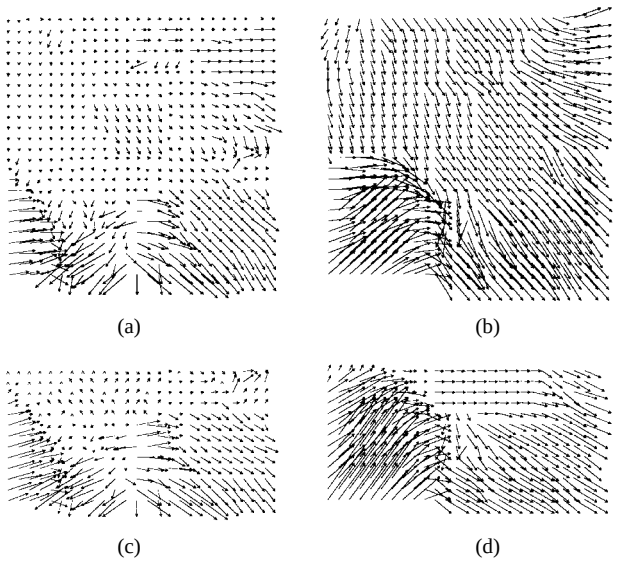

Fig. 15. The optical flows of relative motion when another vehicle is overtaking the vehicle: (a) and (b) are raw optical flows, and (c) and (d) are corrected optical flows.

B. Segmentation of Obstacles

Even if not accurate, the optical flow can be used for a rough segmentation of obstacles and the detection of other moving vehicles in the scene. This can be obtained by subdividing the lower part of the image in small squares (8×8 or 10×10 pixels) and computing for each square a local estimate of V with (16). Connected regions composed by neighboring squares where the absolute value of the difference between the local estimate V_{local} and the best estimated speed V_{best} (computed as in Section IV-B2) is larger than a fixed threshold are labeled as presumed obstacles.

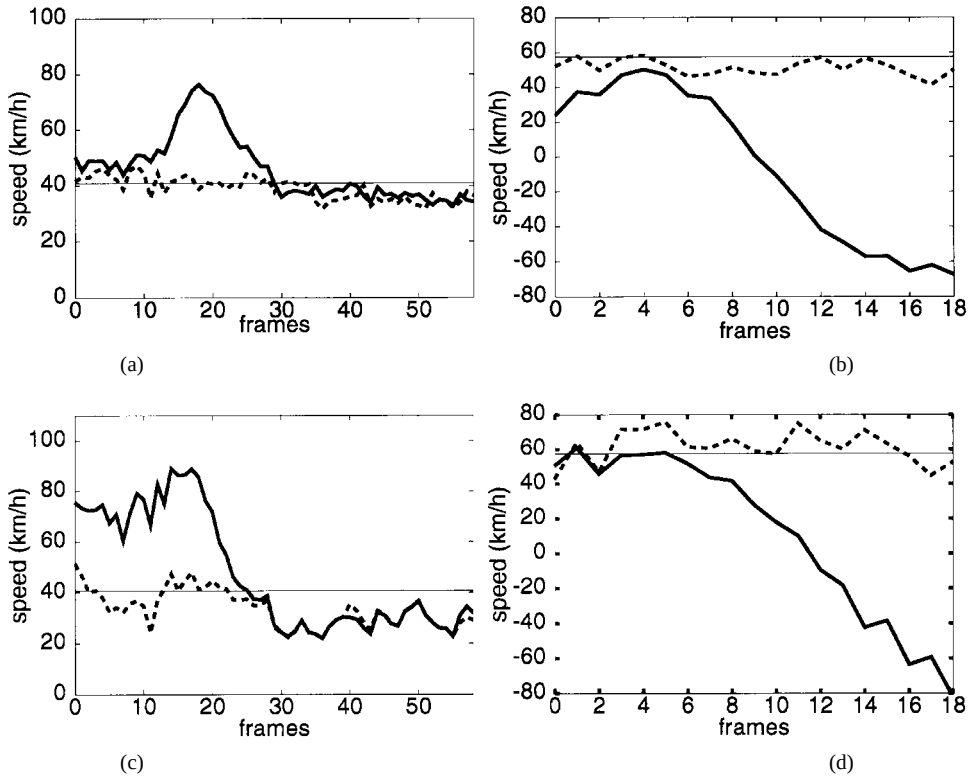

Fig. 16. Estimation of the instantaneous speed V in the left (solid lines) and right region (broken lines). Data in (a) and (c) were obtained from the flows of Fig. 14, those in (b) and (d) from the flows of Fig. 15. Method 1 and 2 were used in the first and second row, respectively. The thin straight line represent the ground truth value.

Fig. 17 shows the result of the region segmentation for an image sequence taken from a car driving on a curvilinear road and overtaken by a faster vehicle. Fig. 17(a) represent a frame of the image sequence and Fig. 17(b) the corresponding optical flow. The output of the speed estimator gives a value of about 30 km/h [broken line of Fig. 17(c)], similar to the ground truth value (thin straight line). The estimate obtained in the left region of the image gives an anomalous negative value (thick line). Fig. 17(d) show the map of the $V_{\text{local}} - V_{\text{best}}$ coded in gray levels: brighter levels correspond to $V > 30$ km/h darker levels to $V < 30$ km/h: the lower-left region of Fig. 20(d) is noticeably darker than the remaining part. The white lines enclose regions with anomalous speed, detected by thresholding the map. Fig. 18 reproduces a similar analysis in the case of a car approaching on the other lane [Fig 18(a)]. As shown in Fig 18(c), the estimated speed in the left region (thick line) is significantly larger than the best estimate, obtained in the right region (broken line). The map of the local speed indicates the presence of an approaching obstacle [Fig. 18(d)]. This segmentation is usually correct far from the horizon, while near the horizon false obstacle detections are often found, because small errors in the optical flow correspond to large variations of V.

C. Localization of Motion Boundaries

When a presumed obstacle is identified with the procedure previously described, it is useful to check whether it is an obstacle or a false alarm caused by the propagation of the optical flow errors in the speed estimate. In addition it is useful to obtain a more precise localization of moving obstacles.

Information obtained from intensity edges can be used to refine the obstacle segmentation (see also [43] and [44]). The procedure is composed by three steps. Firstly, contours of anomalous regions are extracted bythresholding the local speed map. Secondly, intensity edge segments in the image are extracted. Finally each contour is allowed to be attracted by the intensity edges in its interior by using a conventional "snake" algorithm, described in the legend of Fig. 19. Intensity edges converging to the central vanishing point are not considered, so as to avoid interference from lane boundaries. If a contour vanishes because it does not find edges in its interior, a false alarm is declared. Fig. 19 and 20 illustrate this procedure. Fig. 19A reproduces the edge map obtained from the image of Fig. 9(a). These edges are approximated with segments [see Fig. 19(b)]. From the low resolution estimate of $V_{\text{local}} - V_{\text{best}}$ a preliminary segmentation is obtained [Fig. 19(c)]. The anomalous regions extracted are indicated by white contours: it is possible to see the presence of a false obstacle detection near the horizon. The obtained regions are used as a starting point for a snake [45] which has to collapse on edge segments in its interior (see legend of Fig. 19 for further details). The white contour in Fig. 19(d) indicates the final localization of motion boundaries: also the shadow of the car is identified as part of the moving obstacle.

Fig. 20 reproduces the results of the segmentation procedure for the overtaking sequence [shown in Fig. 9(c) and (d)]. Fig. 20(a) reproduces the edge map obtained from the image of

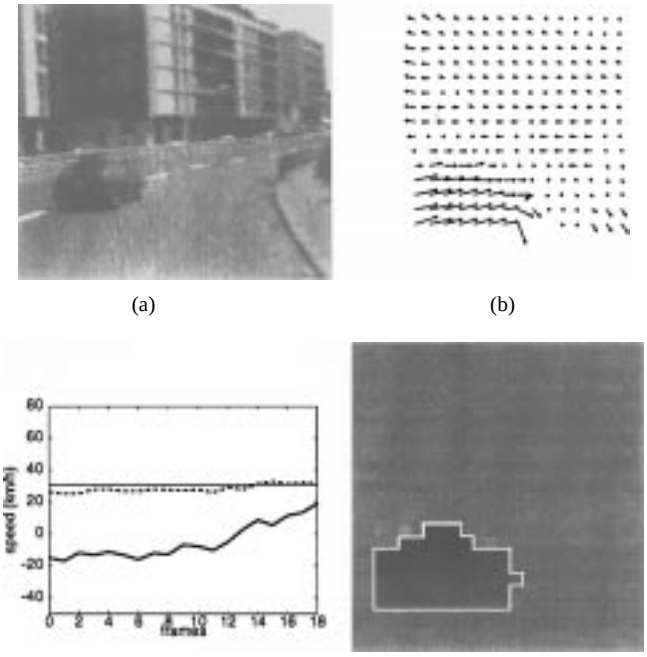

Fig. 17. (a) Sequence image with an overtaking car, (b) corresponding optical flow, (c) best speed estimate, after filtering and rejection of unreliable data vectors (broken line) is close to the instrumentation value (thin straight line). The estimate obtained on the left presents anomalous negative values (thick line), and (d) map of $V_{\rm local} - V_{\rm best}$, where $V_{\rm local}$ was obtained as $(v_y hf/y^2 - \omega hx/y)$ and $V_{\rm best}$ was computed as in Section IV-B2. The difference $V_{\rm local} - V_{\rm best}$ is coded in gray levels. A darker color correspond to lower or negative speed. The white line represents the the contour of a potential obstacle.

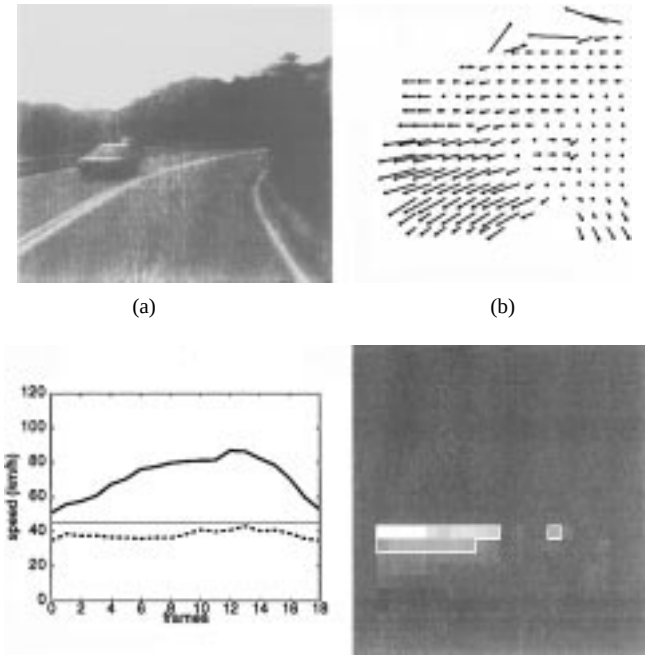

Fig. 18. (a) Sequence image with an approaching car, (b) corresponding optical flow, (c) best speed estimate, after filtering and rejection of unreliable data vectors (broken line) is close to the ground truth value (thin straight line). The estimate obtained on the left presents anomalous high values (thick line), and (d) map of $V_{\rm local} - V_{\rm best}$ obtained as described in Fig. 17.

Fig. 9(c), while only segments not pointing toward the central vanishing point are considered in Fig. 20(b). Fig. 20(c) illustrates the estimates of $V_{\rm local} - V_{\rm best}$. By using the procedure described above the object circled with the white contour in Fig. 20(d) was identified.

VI. Discussion

This paper shows how to obtain a reliable optical flow from road image sequences, from which it is possible to extract relevant information. In order to do so, however, it is necessary to overcome some problems. Firstly, in order to obtain a dense and reliable flow it is necessary to use correlation based techniques, instead of usual differential techniques. Lack of texture and mechanical disturbances make the computation of temporal and spatial derivatives highly unstable (see Section II). Secondly it is necessary to eliminate these mechanical disturbances, either by some stabilization technique [41], [42] or by compensation for shocks and vibrations. When dense and corrected optical flows are obtained, it is possible to recover egomotion parameters (see Section IV) and the presence of relative motions (see Section V).

A. The Recovery of the Egomotion Parameters

The recovery of structure and motion from image sequences is a classical problem of Computer Vision and has inspired a vast literature. A typical approach is based on the solution of a system of equations relating displacements of a sufficient number of image points (or motion field at a single point with first and second order derivatives) to a set of motion and structure parameters [46], [47]. Another approach is to link the derivatives of the image intensity $E(x, y, t)$ directly to the motion parameters [48], [49]. The application of these procedures on real image sequences is rather limited and, in order to have reliable results, displacements must be known with an accuracy larger than 99% [50], [51]. The use of multi-frame approaches, based on Extended Kalman Filters has been proposed [50], [52], but applications of these general techniques to the real world still seem difficult. For practical purposes easier solutions might be found, specific for the particular kind of image and motion. Algorithms working well on real images and noisy optical flows recover only limited or qualitative information, for example the localization of the FOE [53], and were able to recover the translational speed for motion along a straight road. This paper addresses the real situation of the recovery of egomotion parameters from image sequences taken by a TV camera mounted on a commercial vehicle moving along usual roads. The approach starts from the simplifying assumption that the 2-D motion field is adequately represented by the simple (7). Given the focal length of the imaging device f and the camera height from the ground h the egomotion recovery consists in the estimation of the two parameters V and ω. These two parameters are estimated from a noisy but dense optical flow, so that the intrinsic error of an individual displacement is averaged over many displacements. The optical flow is computed by a correlation procedure so as to avoid the instability of computing derivatives. The final estimates of V and ω require some temporal filtering, as

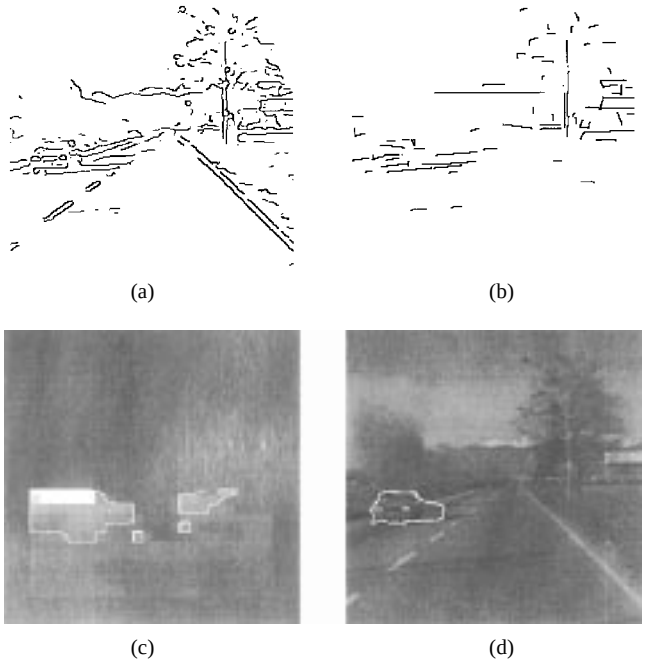

Fig. 19. (a) The edge map obtained from the image of Fig. 9(a) with the procedure of Ottonello *et al.* [56], (b) edge segments from the edge map (a) not pointing toward the central vanishing point, (c) low resolution map (26×14) of $V_{\mathrm{local}} - V_{\mathrm{best}}$. The map has 256 gray levels with white corresponding to an estimated speed of 80 km/h or more and black corresponding to an estimated speed of -80 km/h or less. White lines represent chains of points $\vec{p}(i)$ surrounding connected regions where the difference between the car speed as estimated from the local optical flow and the best value for egomotion is above a given threshold. These white lines are the starting positions of a *snake* [45]. After the initialization, each *snake* undergoes an evolution driven by an elastic force $F_{el} = -\alpha(\vec{p}(i+1)+\vec{p}(i-1)-2\vec{p}(i))$, whose action tends to shrink the contour. The evolution of the points $\vec{p}(i)$ stops when the location of an edge segment has been reached or when the elastic force becomes zero, and (d) white line superimposed to the original image illustrates the detection of the relative motion using the snake.

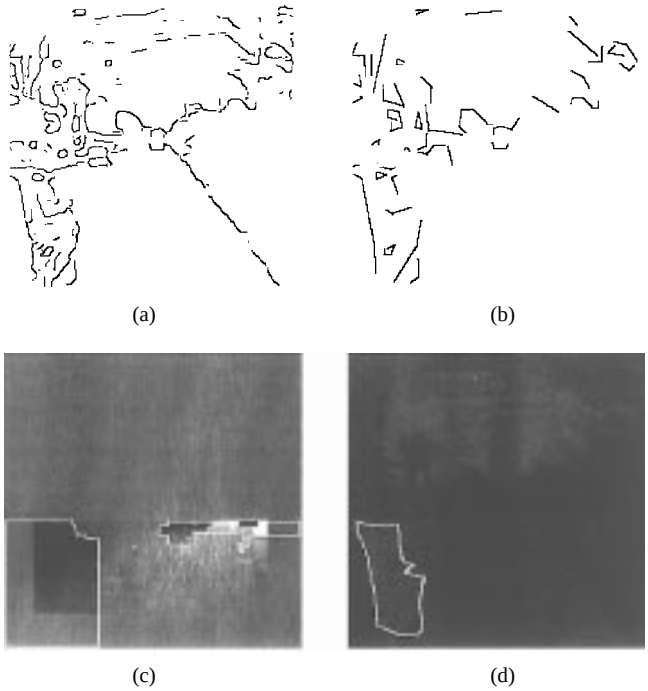

Fig. 20. (a) The edge map obtained from the image of Fig. 9(c), (b) edge segments from the edge map (a) not pointing toward the central vanishing point, (c) low resolution map (26×14) of V (see legend of Fig. 19 for more details), and (D) white line superimposed to the original image indicates the detection of the relative motion. No relative motion was detected in the right part of the image [see (c)] because the snake did not find any segment in its interior.

described in Section IV-C. The experimental results indicate that the speed estimates are highly correlated with ground truth data. These results show that quantitative information can also be recovered from noisy optical flows obtained from image sequences acquired by an imaging device mounted on a vehicle moving along usual roads.

B. The Detection of Relative Motions

Obstacle detection by using optical flow has been already proposed [18]–[21], [55]. The optical flow, by using a special hardware, can be computed in real time [55]. Our procedure for the detection of relative motion occurs in two steps: firstly the presence of a relative motion is established and a coarse segmentation of the optical flow is performed. Secondly, motion discontinuities are better localized by considering also information from intensity edges. The experimental results are satisfactory; the use of model based techniques may provide an even more precise segmentation.

C. Sources of Error and Limitations of the Proposed Technique

The estimation of egomotion parameters, here proposed, is based on the reliability of the optical flow and on the assumption that the expected motion field is described by (7). As a consequence the major sources of errors consist in a poor recovery of optical flow and in a substantial deviation of the true motion field from that of (7).

1) The Computation of Optical Flow: In the presence of shocks and vibrations, caused by the mechanical instability of the viewing camera, a high frequency noise is introduced (see Fig. 6) in the images intensity profile $E(x, y, t)$, so that computing temporal derivatives greatly amplifies noise. As a consequence differential techniques 2[6] do not provide reliable and dense optical flows (see Fig. 2). In order to compute a reliable optical flow correlation based techniques must be used. A recent analysis of obstacle detection with optical flow [55] from similar road image sequences has shown that differential techniques provide reliable results only on very few points of the image. This observation is in agreement with the conclusion that in order to obtain a dense optical flow correlation techniques with large masks must be used. The optical flow obtained with the correlation technique is certainly not exact, but our estimates of the egomotion parameters, i.e. speed and angular velocity, are obtained by averaging over at least 200 individual displacements, significantly reducing the error of an individual displacement. Temporal filtering of the estimates further reduces the error.

2) Shocks and Vibrations: A major problem encountered in the analysis of these image sequences was the presence of disturbances due to shocks and vibrations during image acquisition. Shocks and vibrations are small when the viewing camera is mounted on high quality antivibrating platforms and the vehicle is moving along usual tarred roads. In this case

the 2-D motion field $\vec{s}$ which is caused by these disturbances can be modeled as a constant flow in which the horizontal component can be neglected (see Sections III-A and IV). A stabilization procedure (see also [41], [42]) based on this model can be introduced to obtain a corrected optical flow with the qualitative structure expected from the egomotion of the vehicle and to recover a variety of information on the egomotion and on the relative motion. In the presence of large disturbances during image acquisition a reliable model for the 2-D motion field of shocks and vibrations is difficultly found and therefore it is not clear how to correct the raw optical flow. These disturbances may originate from the bumpiness of the road, the vibrations produced by the vehicle engine and lastly from the driver's temperament. As a consequence these disturbances have different correlation functions and cannot be unequivocally modeled. In this case, however, the egomotion parameters can be estimated from the raw optical flow and some filtered estimates of the instantaneous and angular speed can be subsequently extracted (see IV-D2).

3) Failure of the Proposed Algorithms: The recovery of the egomotion parameters will be successful when (7) describes reasonably well the true motion field. The true motion field is expected to deviate substantially from (7) when the viewed landscape is not perpendicular to the image plane of the TV camera and in the presence of several objects with a significant relative motion. This will be the case when the vehicle moves through a hilly road and dense vegetation. However, the 2-D motion field obtained while moving on a flat and large highway can be satisfactorily described by (7). The proposed technique will evidently fail when the vehicle moves in a cluttered environment with parked cars, people or trees close to the road and many vehicles overtaking or approaching on the other lane.

D. Concluding Remarks

The results presented in this paper show that it is possible to compute a useful optical flow from road image sequences. From this optical flow relevant information for road navigation can be obtained. Similar information can be recovered with other computer vision algorithms; for example, egomotion parameters can be computed with simpler procedures when clear landmarks, such as road markers, are present in the scene. The major requirement for the recovery of a reliable optical flow is the presence of enough texture in the images. Well defined structures and high contrasts are not necessary. As a consequence, the optical flow can be computed in a variety of different scenarios and this versatility appears to be the major advantage of the proposed approach.

ACKNOWLEDGMENT

The authors would like to thank M. Zanini for typing the manuscript and L. Giovanelli for checking the English.

REFERENCES

[1] E. D. Dickmanns and B. D. Mysliewitz, "Recursive 3-d road and relative ego-state recognition," *IEEE Trans. Pattern. Anal. Machine Intell.*, vol. 14, pp. 199–213, 1992.

[2] C. Brudigam, D. Dickmanns, F. Thomanek, E. D. Dickmanns, R. Behringer, and V. V. Holt, "An all-transputer visual autobahn-autopilot/copilot," in *Proc. 4th Int. Conf. Comput. Vision*, 1993, pp. 608–615.

[3] V. Graefe, "Vision for intelligent road vehicles," in *Proc. IEEE Symp. Intell. Veh. '93*, 1993, pp. 135–141.

[4] D. Dickmanns, T. Hildebrandt, M. Maurer, F. Tomanek, E. D. Dickmanns, R. Beringer, and J. Schielen, "The seeing passenger car vamors-p," in *IEEE Symp. Intell. Veh. '94*, 1994, pp. 68–73.

[5] B. Ulmer, "Vita ii—active collision avoidance in real traffic," in *Proc. IEEE Symp. Intell. Veh. '94*, 1994, pp. 1–6.

[6] A. Suissa, U. Franke, S. Mehring, and S. Hahn, "The daimler-benz steering assistant—a spin-off from autonomous driving," in *IEEE Symp. Intell. Veh. '94*, 1994, pp. 120–124.

[7] T. Kanade, C. Thorpe, M. Herbert, and S. Shafer, "Vision and navigation for the carnegie-mellon navlab," *IEEE Trans. Pattern Anal. Machine Intell.*, vol. 10, pp. 361–372, 1988.

[8] ———, "The new generation system for the CMU navlab," in *Vision-based Vehicle Guidance*, I. Masaki, Ed. 1990, pp. 30–82.

[9] K. Gremban, M. Turk, D. Morgenthaler, and M. Marra, "Vits—a vision system for autonomous land vehicle navigation," *IEEE Trans. Pattern Anal. Machine Intell.*, vol. 10, pp. 342–361, 1988.

[10] V. Graefe and K. D. Kuhnert, "Vision-based road autonomous vehicles," in *Vision-based Vehicle Guidance*, I. Masaki, Ed. 1990, pp. 1–29.

[11] S. Dickinson, L. S. Davis, D. DeMenthon, and P. Veatch, "Algorithms for road navigations," in *Vision-based Vehicle Guidance*, I. Masaki, Ed. 1990, pp. 83–110.

[12] M. Nashman and H. Schneiderman, "Real-time visual processing for autonomous driving," in *Proc. IEEE Symp. Intell. Veh. '93*, 1993, pp. 373–378.

[13] J. S. Lee, J. H. Han, K. I. Kim, S. Y. Oh, and C. N. Lee, "An autonomous land vehicle: Design concept and preliminary road test results," in *IEEE Symp. Intell. Veh. '93*, 1993, pp. 146–152.

[14] T. Suzuki, T. Yokoyama, A. Tachibana, and H. Inoue, "Automated vehicle system using both a computer vision and magnetic field sensors," in *Proc. IEEE Symp. Intell. Veh. '93*, 1993, pp. 157–162.

[15] J. Satonobu, K. Kojima, T. Morita, H. Takahashi, and Y. Morimoto, "An approach to the intelligent vehicle," in *Proc. IEEE Symp. Intell. Veh. '93*, 1993, pp. 426–431.

[16] G. W. Zhao and S. Yuta, "Obstacle detection by vision system for an autonomous vehicle," in *Proc. IEEE Workshop Appl. Comput. Vision*, 1993, pp. 31–36.

[17] S. Carlsson and J-O Eklundh, "Object detection using model-based prediction and motion parallax," in *Vision-based Vehicle Guidance*, I. Masaki, Ed. 1990, pp. 148–161.

[18] R. C. Nelson and Y. Aloimonos, "Obstacle avoidance using flow field divergence," *IEEE Trans. Pattern Anal. Machine Intell.*, vol. 11, pp. 1102–1106, 1989.

[19] W. Enkelmann, "Obstacle detection by evaluation of optical flow fields," in *Proc. 1st Euro. Conf. Comput. Vision*, 1990.

[20] T. Ito and S. Kawakatsu, "An extracting method of the optical flow for an anticollision system," in *Vision-based Vehicle Guidance*, I. Masaki, Ed. 1990, pp. 255–267.

[21] M. Herman, G.S. Young, T-H. Hong, and J. C. S. Yang, "New visual invariant for obstacle detection using optical flow induced from general motion," in *Proc. IEEE Workshop Appl. Comput. Vision*, 1992, pp. 100–109.

[22] B. K. P. Horn and B. G. Schunck, "Determining optical flow," *Artif. Intell.*, vol. 17, pp. 185–203, 1981.

[23] E. C. Hildreth, "The computation of the velocity field," in *Proc. Roy. Soc. Lond. B*, vol. 221, pp. 189–220, 1984.

[24] H. H. Nagel, "Displacement vectors derived from 2nd order intensity variations in image sequences," *Comput. Vis. Graph. Image Processing*, vol. 21, pp. 85–117, 1983.

[25] D. J. Heeger, "Optical flow using spatio-temporal filters," *Int. J. Comput. Vis.*, vol. 2, pp. 279–302, 1988.

[26] F. Girosi, A. Verri, and V. Torre, "Differential techniques for optical flow," *J. Opt. Soc. Amer. A*, vol. 7, pp. 912–922, 1990.

[27] D. J. Fleet, J. L. Barron, and S. S. Beauchemin, "Performance of optical flow techniques," *Int. J. Comput. Vis.*, vol. 12, pp. 43–77, 1994.

[28] M. Otte and H. H. Nagel, "Optical flow estimation: advances and comparisons," in *Proc. 4th Euro. Conf. Comput. Vision*, J-O Eklundh, Ed., 1994.

[29] A. Giachetti, M. Campani, R. Sanni, and A. Succi, "The recovery of optical flow for intelligent cruise control," in *Proc. IEEE Symp. Intell. Veh. '94*, 1994, pp. 91–96.

[30] A. Giachetti, M. Campani, and V. Torre, "The use of optical flow for the autonomous navigation," in *Proc. 4th Euro. Conf. Comput. Vision*, J.-O. Eklundh, Ed., 1994.

[31] E. C. Adelson and J. R. Bergen, "Spatiotemporal energy models for the perception of motion," *J. Opt. Soc. Amer. A*, vol. 2, pp. 284–299, 1985.
[32] P. Anadan, "A computational framework and an algorithm for the measurement of visual motion," *Int. J. Comput. Vis.*, vol. 3, pp. 283–310, 1989.
[33] D. J. Fleet and A. D. Jepson, "Computation of component image velocity from local phase information," *Int. J. Comput. Vis.*, vol. 5, pp. 77–104, 1990.
[34] M. Campani and A. Verri, "Motion analysis from first order properties of optical flow," *Comput. Vis. Graph. Image Processing—Image Understanding*, vol. 56, pp. 90–107, 1992.
[35] A. Verri and T. Poggio, "Against quantitative optical flow," in *Proc. 1st Int. Conf. Comput. Vision*, 1987, pp. 171–180.
[36] F. Girosi, A. Verri, and V. Torre, "Mathematical properties of the two-dimensional motion field: from singular points to motion parameters," *J. Opt. Soc. Amer. A*, vol. 6, pp. 698–712, 1989.
[37] M. Straforini, A. Verri, and V. Torre, "Computational aspects of motion perception in natural and artificial vision system," *Trans. Roy. Soc. Lond. B*, vol. 337, pp. 429–443, 1992.
[38] S. Uras, E. De Micheli, and V. Torre, "The accuracy of the computation of optical flow and of the recovery of motion parameters," *IEEE Trans. Pattern Anal. Machine Intell.*, vol. 15, pp. 434–447, 1993.
[39] A. Giachetti and V. Torre, "Refinement of optical flow computation and detection of motion edges," in *Proc. ECCV '96*, Cambridge, MA, 1996.
[40] E. De Micheli and A. Verri, "Vehicle guidance from one dimensional optical flow," in *Proc. IEEE Symp. Intell. Veh. '93*, 1993.
[41] J. R. Bergen, P. Anandan, K. J. Hanna, and R. Hinograni, "Hierarchical model-based motion estimation," in *Proc. ECCV '92*, Santa Margherita, 1992, pp. 237–252.
[42] M. Irani, B. Rousso, and S. Peleg,"Computing occluding and transparent motions," *Int. J. Comput. Vis.*, vol. 12, no. 1, pp. 5–16, 1994.
[43] F. Heitz and P. Bouthemy, "Multimodal estimation of discontinuous optical flow using markov random fields," *IEEE Trans. Pattern Anal. Machine Intell.*, vol. 15, pp. 1217–1232, 1993.
[44] E. Francois and P. Bouthemy, "Motion segmentation and qualitative dynamic scene analysis from an image sequence," *Int. J. Comput. Vis.*, vol. 10, pp. 157–182, 1993.
[45] A. Witkin, A. Kass, and D. Terzopoulos, "Snakes: Active contour models," *Int. J. Comput. Vis.*, vol. 1, pp. 321–331, 1988.
[46] H. C. Longuet-Higgins and K. Prazdny, "The interpretation of moving retinal images," in *Proc. Roy. Soc. Lond. B*, vol. 223, pp. 165–175, 1981.
[47] R. Y. Tsai and T. S. Huang, "Uniqueness and estimation of three-dimensional motion parameters of rigid objects with curved surfaces," *IEEE Trans. Pattern Anal. Machine Intell.*, vol. 6, pp. 13–27, 1984.
[48] S. Negahdaripour and B. K. P. Horn, "Direct passive navigation," *IEEE Trans. Pattern Anal. Machine Intell.*, vol. 9, pp. 168–176, 1987.
[49] B. K. P. Horn and E. J. Weldon, "Direct methods for recovering motion," *Int. J. Comput. Vis.*, vol. 2, pp. 51–76, 1988.
[50] M. E. Spetsakis and J. Aloimonos, "Multi-frame approach to visual motion perception," *Int. J. Comput. Vis.*, vol. 6, pp. 245–255, 1991.
[51] A. Jepson, J. L. Barron, and J. Tsotsos, "The feasibility of motion and structure from noisy time-varying image velocity information," *Int. J. Comput. Vis.*, vol. 5, pp. 239–269, 1990.
[52] R. Frezza, S. Soatto, P. Perona, and G. Picci, "Recursive motion and structure estimation with complete error characterization," in *Proc. IEEE Conf. Comput. Vision Pattern Recognition*, 1993, pp. 428–433.
[53] Y. Aloimonos and Z. Duric, "Active egomotion estimation: A qualitative approach," in *Proc. 2nd Euro. Conf. Comput. Vision*, 1992, pp. 497–510.
[54] M. Campani, M. Straforini, A. Malisia, A. Baghino, and V. Torre, "The use of optical flow for the autonomous navigation," *Int. J. Neural Syst.*, vol. 3, pp. 121–137, 1992.
[55] W. Kreger, S. Rossle, W. Enkelmann, V. Gegenbach, and W. Tolle, "Obstacle detection by real-time optical flow evaluation," in *IEEE Symp. Intell. Veh. '94*, 1994, pp. 97–102.
[56] P. Ottonello, E. De Micheli, B. Caprile, and V. Torre, "Localization and noise in edge detection," *IEEE Trans. Pattern Anal. Machine Intell.*, vol. 11, pp. 1106–1117, 1989.

Andrea Giachetti was born in Savona, Italy, on February 7, 1968. He received the Ph.D. degree in theoretical physics from the University of Genova, Italy, in 1993.

From 1993 to 1997, he worked at the Department of Physics, University of Genova on the problems concerning the analysis of motion in machine vision and in biomedical imaging. Since 1997, he has been enployed at the CRS4 (Center for Advanced Studies, Research and Development, Sardinia) where he is working on the development of new techniques for biomedical imaging.

Marco Campani was born in Genova, Italy, on October 5, 1961. He received the Ph.D. degree in theoretical physics from the University of Genova, Italy, in 1990.

From 1986 to 1996, he worked at the Department of Physics, University of Genova on problems concerning signal processing and motion analysis in machine vision. From 1992 to 1996, worked at the Genova Research Unit, "Istituto Nazionale per la Fisica della Materia" on various aspects of image analysis and processing. Since 1996, he has been working at the Department of Physics, University of Genova, where he is mainly involved in problems concerning digital networks and distributed computing systems.

Vincent Torre was born in Johannesburg, South Africa, on July 24, 1950. He received the Ph.D. degree in theoretical physics from the University of Genova, Italy, in 1973.

From 1974 to 1978, he worked on the electrophysiology of retinal cells at the Laboratory of Neurophysiology, CNR, Pisa, Italy. From 1979 to 1981, he worked on the mechanisms of phototransduction at the Physiological Laboratory, Cambridge, U.K. Since 1991, he has been Full Professor in Cybernetics and Information Theory. He is working on information processing in man and machine at the ISAS (International School for Advanced Studies), Trieste, Italy.